Atomistic understanding of ion-exchange strengthening of boroaluminosilicate glasses: insights from Molecular Dynamics simulations and QSPR analysis

Po-Hsuen Kuo, Jincheng Du*

Department of Material Science and Engineering, University of North Texas, Denton, Texas, 76203, USA

(*Corresponding author. Email: du@unt.edu)

Abstract

Ion exchange (IOX) is an effective and widely used method to enhance mechanical properties of various glass products ranging from touch screen of consumer electronics to window shields of airplanes and spacecrafts. IOX or chemical strengthening is achieved through the creation of a compressive surface layer on the glass product. Although widely studied experimentally, fundamental understanding of the ion-exchange strengthening process is still limited. In this work, we have applied large scale atomistic simulations to understand ion-exchange induced mechanical property changes and their relation to the glass composition and structural characteristics. Two series of borosilicate glasses are studied to elucidate the effects of composition effect, including boron oxide to silica and alumina to silica substitutions and different levels of K⁺ to Na⁺ exchanges, on the mechanical properties by using molecular dynamic (MD) simulations with a set of recently developed effective partial charge potentials. Linear network dilation coefficient (LNDC), a common measure of IOX behaviors, were calculated for each of the glass compositions. Quantitative structural property relationship (QSPR) analysis based on the MD generated structural features was used to establish structure-property correlations of mechanical and other properties. The results show strong composition dependence of LNDC hence suitability of IOX strengthening and this behavior is discussed based on glass structure features. Glass compositions with higher amount of mixed glass formers, higher network connectivity, and

less complex components tend to show higher calculated LNDC and higher surface compressive stress. MD simulations, in combination with QSPR analysis, can thus provide atomistic insights on how glass composition and structure characteristics affect ion exchange behaviors.

Key words: ion-exchange process, chemical strengthening, molecular dynamics, QSPR, borosilicate glass, boroaluminosilicate glass, mechanical properties

1. Introduction

The ion exchange (IOX) process, or chemical strengthening, has been widely used in the glass industry and advanced technologies to enhance the strength and toughness of glass products ever since its first development in early 1960s. Unlike conventional thermal strengthening, IOX can be applied to ultra-thin glass products and has high dimensional tolerance thus leads to numerous applications ranging from touch screens in consumer electronics, aerospace and highspeed train windshields, ophthalmic glass, and substrate of hard drive for information storage and electronic circuits ^{2–5}. IOX, also known as ion exchange stuffing, chemical tempering or chemical strengthening, is a surface modification process that involves thermally-activated interdiffusion of alkali ions between the glass and the molten salt bath. Larger cations (such as K⁺) from the molten salt diffuse into the surface layer of the glass, exchanging with smaller cations (such as Na⁺) from that glass that diffuse out to the molten salt, creating a compressive surface layer that improves the mechanical strength of the glass product. The temperature of IOX process is usually kept below the glass transition temperature (Tg) to reduce stress relaxation that can reduce the strengthening effect. Typically, IOX can generate tens to hundreds of microns thick compressive layer, leading to several hundred MPa surface compression. 6 This surface compressive stress layer can prevent crack imitation and propagation when encountering external impacts, hence improving the strength and damage resistance, of the glass products. Despite wide spread industrial applications, the exact mechanism of the ion-exchange strengthening mechanisms is still not fully understood, due to the lack of suitable in-situ characterization methods to probe the structural changes and stress developments during the IOX process. This lack of understanding makes it challenging to rationally design of new glass compositions for IOX processing and applications. Atomistic simulation methods such as molecular dynamics, which have already been widely adopted to study glass structures, however, can potentially address these challenges and to provide insights of insitu structural changes at atomic scale during the IOX processes in glasses. Recently, the simulation and modeling based materials genome approaches have been used to accelerate the development of various types of materials. In this study, we aim to combine physics based atomistic simulations and data-driven technique such as QSPR analysis as a new approach to understand the IOX processes and associated mechanisms with a goal to gain insights on how glass composition and structures affect the effectiveness of the IOX processes.

The mathematical expression of stress profile generated by IOX can be shown by Eq. (1)

$$\sigma(z) = -\frac{BE}{1-\nu} [C(z) - C_{avg}] \quad --(1)$$

where $\sigma(z)$ is the compressive stress at the penetration depth z, reached by the alkali ion during IOX process, E is the Young's modulus of the glass, v is the Poisson's ratio. Equation 1 does not take into consideration of stress relaxation. For the force balance condition, the average concentration of substituting alkali ion concentration, C_{avg} , is subtracted from the local concentration of substituting alkali ion, C(z), allowing the net stress to be zero. i.e. the integration of compressive stress from the surface to the maximum penetration depth is compensated by the tensile stress, therefore resulting in a zero internal stress. The parameter B is the linear network dilation coefficient (LNDC), which is also known as the "Cooper coefficient" ^{7,8}. LNDC gives the linear strain per unit change of alkali ion concentration, which can be expressed as

$$B = \frac{1}{3} \left(\frac{1}{V} \frac{\partial V}{\partial C} \right) \qquad ---(2)$$

where the factor $\frac{1}{3}$ is converting the volume coefficient to linear coefficient of thermal expansion for isotropic materials, V is the volume of the glass, and C is the concentration of IOX. By combining Eq (1) and (2) above, $-\frac{E}{1-v}$ can be considered as a factor that converts B, the strain caused by IOX (LNDC), to the stress induced by IOX in the glass. By ignoring the stress relaxation contribution, the compressive stress is directly proportional to the strain induced by per unit of IOX concentration.

In the early studies, it was found that the value of the linear network dilation coefficient (*B*) calculated from the Eq (2) is 2 to 4 times higher than that derived the Eq (1) (with the value of $\sigma(z)$, C(z), E and v from experimental measurement). For example, in 15Na₂O-10CaO-75SiO₂ glass with Na⁺ \leftrightarrow K⁺ IOX, the calculated $B \approx 1.3 \times 10^{-3} ([\text{mol}\% \text{ K}_2\text{O}^{-1}])$, whereas the experimental measured $B \approx 3 \sim 6 \times 10^{-4} ([\text{mol}\% \text{ K}_2\text{O}^{-1}])$. This discrepancy between experimentally-measured and

theoretically calculated B results in lower stress profile in IOX glasses than what the model predicted. Because the IOX temperature is significantly lower than T_g, the discrepancy cannot be easily explained by the viscous relaxation of glass ^{4,7–14}. By adopting molecular dynamic (MD) simulations, it has now been found that this network dilation anomaly can be explicated by the short and medium range atomic structures of glass. Varshneya et al. 4,9,10,15,16, Mauro et al. 12,14,17, and Tandia et al. 18,19 detected that the anomaly can also be contributed by the atomic structural rearrangement. Tandia et al. showed that the change of local environment of cations affects the value of LNDC. During Na $^+\leftrightarrow$ K $^+$ IOX process, K $^+$ quickly move into a higher K-O coordination but without commensurate molar volume change, volume strain comparing to compositional equivalent as-melted (CEAM) K⁺-stuffed glass. The volume difference between two glasses generated from IOX process and melt-and-quench process create an elastic strain that introduced the stress within glass of same composition. Tandia et al. described the IOX glass and the CEAM glass as two different glasses with the same composition but acquired through two different types of relaxation process 18,20. After salt bath, the volume of IOX glass expand elastically and delay elastically by the fast "β-relaxation", allowing larger ions to accommodate into glass structure without altering the major Si-O network in glass structure. The volume of CEAM glass expands much slower by the "α-relaxation", which requires higher temperature for glass network viscous flow 4,11,12,15,18. The results show a strong connection between the mechanical and structural properties of glass and the local environment change of major alkali ions, K and Na. As most of investigations were done in as silicate glasses or aluminosilicate glasses, such as Na₂O-K₂O-SiO₂, Na₂O-K₂O-Al₂O₃-SiO₂ or Na₂O-CaO-SiO₂, it is worth to explore more complicated compositions with multiple glass former. By using MD simulation, this paper estimated the effectiveness of mechanical properties enhancement by IOX in borosilicate and aluminoborosilicate glasses.

Quantitative Structure Property relationship (QSPR) analysis is an approach to build the correlation between the pre-determined structural descriptors of a material and its properties. By establishing the statistical relationship between one or multiple predefined descriptors and the targeted properties of the material, the mathematical relationship can be established ²¹. The mathematical relationship can be considered as a guidance for inverse design the material composition or processing method to achieve the desired properties predicted by the QSPR analysis ^{21–24}. Combing the vast amount of research data accumulated throughout the history and the thriving data-analysis method in recent years, QSPR analysis has become increasingly

economical and feasible comparing to the conventional trail-and-error exploration of material development. With growing number of mathematical relationships being discovered; the desired function can be reached with less raw material and lab hour. For example, using different descriptors, QSPR analysis has been proven to be successful in predicting the properties of polymer material, e.g., glass transition temperature $(T_g)^{23-26}$, bioactivity 22,27 , and tensile modulus 28 . In the glass field, Lusvardi et al. discovered that by using the theoretical structural descriptor $(F_{\rm net})$, QSPR analysis can also be used to predict the properties of silica-based and phosphor-silicate-based bioactive glass, such as crystallization temperature (T_c) , T_g and bioactivity $^{29-32}$. Our recent studies expanded the adoptability of QSPR analysis and MD simulation calculated $F_{\rm net}$ of the multicomponent glass with strong network formers, such as Zr and B. The result shows that the $F_{\rm net}$ gives excellent linear relationship with the density, T_g and the dissolution rate (r_0) measured by experiment approaches $^{33-35}$. The well agreement suggests a great potential of an economic approach of function-oriented compositional design of the multicomponent glass. Therefore, correlation of mechanical properties and composition of glass can be established by QSPR and find the optimal condition.

In this work, we chose two series of multi-component glass compositions boroaluminosilicate glasses (named as NQ and ISG series) and substituted the major glass former SiO₂ with Al₂O₃+Na₂O and B₂O₃+Na₂O, respectively. The six component ISG glass, developed as a model system to study the chemical durability in the field of nuclear waste disposal, was chosen due to the fact that it has been widely investigated and detailed structural and property information such as mechanical and chemical durability are available. The NQ series are basically sodium borosilicate glasses with addition of alumina. These two glass series provide a base of comparison of more complex versus simpler compositions, as well as the effect of glass former mixing as a result of the substitutions, on the glass structures and ion-exchange efficiency. After the regular melt-and-quench generation of the bulk glass structures in each of the glass compositions, 20%, 40%, 60% and 80% of Na⁺ ions were substituted by of K⁺ ion as a simulation of the IOX process. Besides the compositional change, the glass was acquired by two methods in MD simulation: (1) Anneal (named as "-an"), to simulate the typical experimental condition of IOX, and (2) Melt-and-quench (named as "-mq"), to simulate CEAM glass. The volume change was acquired after proper equilibrium in MD simulation and the Young's Modulus and stress profile of glasses were acquired by micro-strain process. The increasing IOX concentration will

be used to represent the glass composition from bulk to surface of IOX. F_{net} of glasses were calculated from the structural analysis and factors based on the previous studies ³³. The influence of glass former substitution and IOX concentration to the mechanical properties and to the structural energy were studied using the QSPR analysis. For best of our knowledge, there is no similar study on the multi-component borosilicate glasses. We hope this paper can provide an insight of IOX in the more complicated glass composition and explore the potential of MD simulation and QSPR analysis.

2. Methodologies

The compositions of two series of glass used in this work, named ISG and NQ, were shown in Table 1 and Table 2, respectively. For ISG series, 5% of SiO₂ in glass was substituted by B₂O₃+Na₂O. The stoichiometric description of ISG series compositions is (60.2+5x)SiO₂-(16.0-2.8x)B₂O₃-(12.6-2.2x)Na₂O-3.8Al₂O₃-5.7CaO-1.7ZrO₂ (x = 1, 0, -1). x = 1, 0, -1 corresponds to ISG-BM, ISG-BO, and ISG-BP, respectively. It is worth mentioning that ISG-BO glass is the nominal compositions of international simplified glass (ISG), which has been deeply investigated since 2013 for its representative characteristics of nuclear waste glass ⁷. As shown in Table 2, 8.2% of SiO₂ was substituted by Al₂O₃+Na₂O. The stoichiometric description of NQ series glass is (65.2+8.2x)SiO₂-12.3B₂O₃-(18.4-4.1x)Na₂O-(4.1-4.1x)Al₂O₃ (x = 1, 0, -1). x = 1, 0, -1 corresponds to NQ-AlO, NQ-AlP and NQ-AlM, respectively. The samples are named based on {glass series name}-{substituent glass former} {"O", "M" or "P"}. The "O", "M" and "P" represents "original glass (x = 0)", "minus substituent (x = 1)" and "plus substituent (x = -1)".

Table 1. Compositions of ISG series glass in molar percentage

Sample	SiO ₂	B_2O_3	Na ₂ O	Al ₂ O ₃	CaO	ZrO ₂
ISG-BM	65.2	13.2	10.4	3.8	5.7	1.7
ISG-BO	60.2	16.0	12.6	3.8	5.7	1.7
ISG-BP	55.2	18.8	14.8	3.8	5.7	1.7

Table 2. Compositions of NQ series glass in molar percentage

Sample	SiO ₂	B_2O_3	Na ₂ O	Al ₂ O ₃
NQ-AIM	73.4	12.3	14.3	0.0
NQ-AIO	65.2	12.3	18.4	4.1

NQ-AIP 57.0 12.3 22.5

2.1 Simulation detail for ISG and NQ series glasses

MD simulation in this study was done by Large-scale Atomic/Molecular Massively Parallel Simulator (LAMMPS)³⁶ with partial effective charge pairwise empirical Buckingham potential.

$$V(r_{ij}) = \frac{q_i q_j e^2}{4\pi\varepsilon_0 r_{ij}} + A_{ij} \exp\left(\frac{-r_{ij}}{\rho_{ij}}\right) - \frac{c_{ij}}{r_{ij}^6}$$
(3)

where V and r_{ij} is the potential energy and interatomic distance between ion i and j, respectively. The first term describes the long-range Coulombic interaction, q_i and q_j are the partial atomic charge of ion i and j and ε_0 is the electrical permittivity in vacuum. The second and third term describe the exponent repulsion the Buckingham form van der Walls attraction energy. The potential parameters, A_{ij} , C_{ij} and ρ_{ij} , used in this study are listed in Table 3, and the detail of the potential development can be found in references by Deng and Du 37,38 . The reason to choose this set of potential is due to its capability to reproduce boron coordination change in wide composition ranges and the availability of compatible potential parameters for all oxides in the two glass series including those for ZrO₂ and K₂O. Each of simulation cell contains approximately 10,000 atoms, basing on the different composition, and 3 parallel tests were done for the each of 6 glass compositions. The initial atomic configuration of ISG and NQ series glasses was generated by randomly placing atoms in a cubic cell. Then the simulation cell was melted at 6000K using canonical ensemble (NVT) for 200 ps, quenched at a rate of 5K/ps using NVT, then equilibrated at 300K using isothermal-isobaric ensemble (NPT), NVT and microcanonical ensemble (NVE) for 100 ps, respectively. The last configuration of NVE equilibrium was used as the as-obtained glass.

Table 3. Atomic charges and Buckingham potential parameters³⁹

Atom Pair (i-j)	A _{ij} (eV)	$ ho_{ij}(ext{Å})$	$C_{ij}(eV \cdot \mathring{A}^6)$
Si ^{2.4} —O ^{-1.2}	13702.905	0.193817	54.681
B ^{1.8} —O ^{-1.2}	14550.972	0.171281	28.500
Na ^{0.6} —O ^{-1.2}	4383.756	0.243838	30.700
Al ^{1.8} —O ^{-1.2}	12201.417	0.195628	31.997
Ca ^{1.2} —O ^{-1.2}	7747.183	0.252623	93.109
Zr ^{2.4} —O ^{-1.2}	17943.394	0.226627	127.650
K ^{0.6} -O ^{-1.2}	20526.972	0.233708	51.489

O ^{-1.2} —O ^{-1.2}	2029.220	0.343645	192.580
--------------------------------------	----------	----------	---------

2.2 MD simulation of ion-exchanged glasses

The mechanical properties of ISG and NQ series glass as a function of IOX concentration was investigated by randomly substituting 20%, 40%, 60% and 80% of Na in the glass with K. These glasses were named as IOXISG and IOXNQ glasses. Two methods, anneal and melt-quench, were used to generate IOXISG and IOXNQ glasses. For anneal method, the IOX glasses was annealed at 700K using NVT for 200 ps, which corresponds to the typical temperature of IOX salt bath in lab. The glass is then quenched at a rate of 5K/ps using NVT and equilibrated at 300K using NPT, NVT and NVE for 100 ps in each ensemble. The last configuration from NVE equilibrium was used as the synthesized glass and named as IOXISG-an and IOXNQ-an glasses. For melt-quench method, the IOX glass goes through the high temperature to achieve full structural relaxation, as described in the previous section. The glass was melted at 6000K for 200 ps, quenched at a rate of 5K/ps using NVT, then equilibrated at 300K using NPT, NVE, and NVE for 100 ps, respectively. The last configuration of NVE equilibrium were used as IOXISG-mq and IOXNQ-mq glasses. The -mq and -an glasses will be used to calculated LNDC (Figure 1).

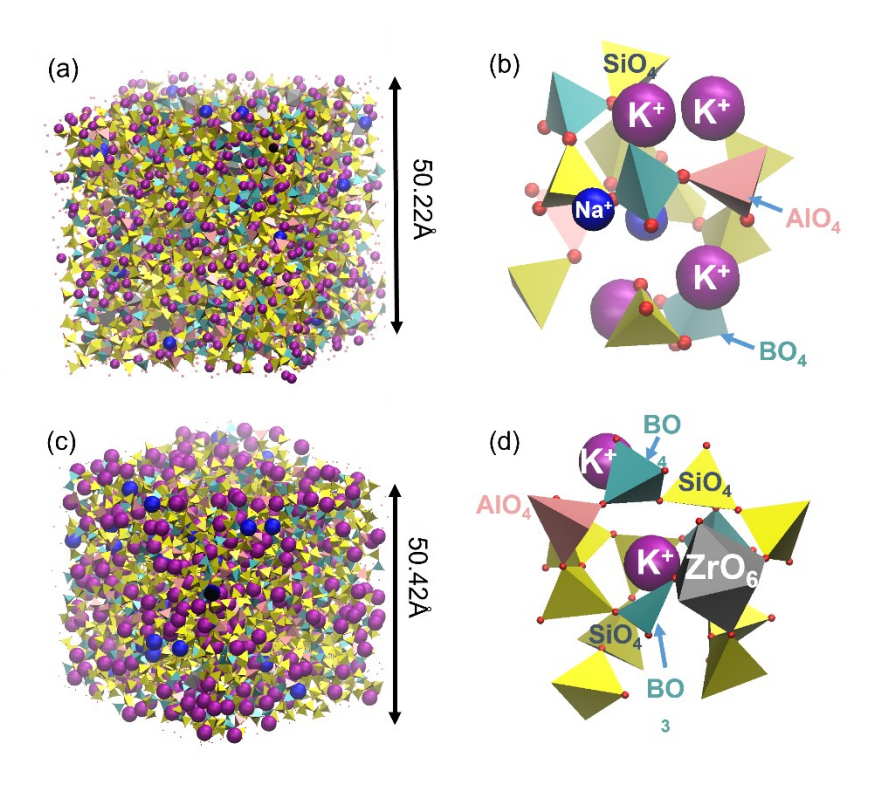


Figure 1 (a) Simulation cell and (b) cation local environment of IOXISG-BM-an with 80% IOX. (c) Simulation cell and (d) cation local environment of IOXISG-BM-mq with 80% IOX

2.3 Mechanical Properties calculations

Mechanical properties, including Young's, bulk, and shear modulus of ISG, NQ, IOXISG, and IOXNQ series glasses, were calculated from the micro strain induced energy change based on energy minimization using a script within LAMMPS developed by Aidan Thompsan ⁴⁰ (Fig. 2). The method was developed for crystalline materials but had been proven to be feasible in the glass systems combining with Buckingham potential by the previous study ⁴¹. It is assumed the system to be isotropic, although minute values of stress components might appear due to finite size of the simulation cell. These values, however, are relatively small. The elastic stiffness tensor, as shown by Eq. (4),

$$\sigma_i = C_{ij} \times \varepsilon_i$$
 (4)

where σ_i are the stress tensor elements, ε_j are the responding symmetric strain tensor elements, and C_{ij} (*i*, and *j* are the Voigt deformation component, which equals to 1, 2, 3, 4, 5, 6)

is the elastic constant tensor. Zero energy minimization method was applied before the deformation. The compliance matrix (S) was later derived from the inverse of elastic constant matrix ($S = C^{-1}$). The compliance and elastic constant matrix were used in Voigt, Reuss and Hill's method to obtain bulk (B) and shear modulus (G). Voigt method is based on the aggregation of uniform strain, as shown in Eq. (5) and (6).

$$B_{Voigt} = \frac{1}{9} (C_{11} + C_{22} + C_{33} + 2(C_{12} + C_{13} + C_{23}))$$
 (5)

$$G_{Voigt} = \frac{1}{15} (C_{11} + C_{22} + C_{33} - (C_{12} + C_{13} + C_{14}) + 3(C_{44} + C_{55} + C_{66}))$$
 (6)

Reuss method is based on the aggregation of the uniform stress, as shown in Eq. (7) and (8).

$$B_{Reuss} = \left(S_{11} + S_{22} + S_{33} + 2(S_{31} + S_{21} + S_{32})\right)^{-1} \tag{7}$$

$$G_{Reuss} = \frac{15}{4(S_{11} + S_{22} + S_{33} - S_{12} - S_{23} - S_{13}) + 3(S_{44} + S_{55} + S_{66})}$$
(8)

The Young's modulus is calculated by Eq. (9).

$$E = \left(\frac{1}{3G} + \frac{1}{9K}\right)^{-1} \tag{9}$$

For the statistical accuracy, the bulk, shear, and Young's modulus reported in this study were calculated from Hill's method, which is the geometric mean of the modulus calculated from Voigt and Reuss methods ⁴². Before calculating the final result of mechanical properties, parameters like numbers of iterations of force/energy minimization and evaluation of each glass compositions were toggled until the convergence of elastic constant tensor (C₁₁, C₂₂, or C₃₃) was reached to ensure the validity of calculation. And the trajectories from 6-directions were examined to ensure no fracture occurs in the simulation box within the deformation process.

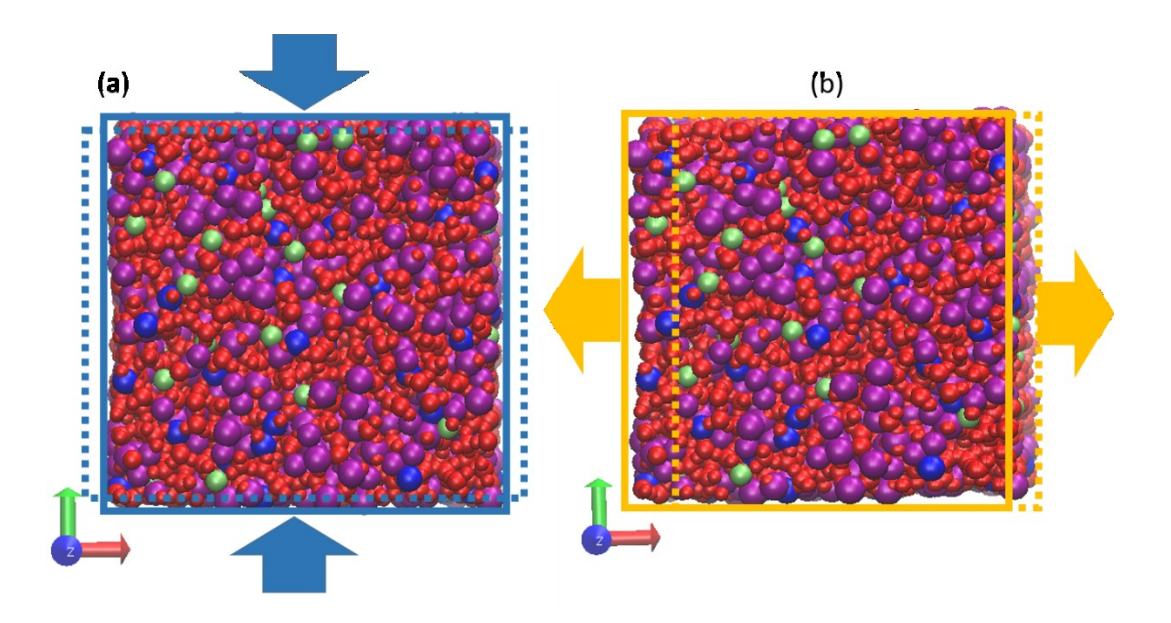


Figure 2 Snapshot of simulation cell and schematics of strain-induced during mechanical property calculation: (a) compressive strain along y-axis (b) shear strain parallel to x-y plane.

2.4 Quantitative Structure and Property Relationship (QSPR) analysis

In this study, we use a structural descriptor (F_{net}) that was first developed by Lusvardi et al.^{30,32} to summarize the structural characteristics and chemical bonding contributions. The descriptor has been used in our earlier work on zirconia effect on borosilicate glasses to describe the density and dissolution rate changes with composition, the thermomechanical properties such as thermal expansion coefficients, hardness and Young's moduli of calcia aluminosilicate glasses, all in combination with structural characteristics from MD simulations. The mathematical expression is shown by Eq. (10).

$$F_{net} = \frac{1}{N_{atoms}} \sum_{x}^{N_{cations}} n_x C N_{xo} SBS_{xo} m_x$$
 (10)

in Eq (10), N_{atoms} is the total number of atoms, $N_{cations}$ is the total number of cations, n_x is the number of cation x (x = Na, Ca, Al, B^[4], B^[3], Si, Zr), CN_{xo} is the average coordination number of "cation x—oxygen pair", SBS_{xo} is the single bond strength from the study by Sun^{43} , and lastly, m_x is the multiplicative factor for each cation—oxygen pair. It is worth noting that the earlier QSPR analysis used bond strength of diatomic molecule or cation but our studies showed the single bond strength by Sun as used for classification of glass formers and modifiers can provide consistent trend in wide ranges of glass compositions and various properties. Hence the single

P-H Kuo, J. Du, J. Phys. Chem. B 2022, 126, 9, 2060-2072

bond strength was used in this work for QSPR analysis of the original and ion-exchanged glasses. Table 4 below summarizes the SBS $_{xo}$ and m_x used in this study.

Table 4 Single bond strength and multiplicative factor of cation-oxygen pairs

Cation-Oxygen pair	Single bond strength (kcals/mol)	m _x (multiplicative factor)
Na-O	20	1
K-O	13	1
Са-О	32	2
$\mathbf{B}^{[3]}$ -O	119	3
Al-O	79	4
B ^[4] -O	89	4
Si-O	106	4
Zr-O	81	6

3 Results

3.1 Influence of composition and synthesis methods to the mechanical properties

In this work, the compositional change includes different levels of glass former substitution and K/Na substitution. The synthesis method includes low temperature annealing (named as "-an") and high temperature melt-and-quench (named as "-mq").

Fig. 3 and 4 show the Young's, bulk and shear modulus calculated of the (IOX)ISG-an and (IOX)ISG-mq glass, respectively. From Fig. 3 and 4, three observations regarding the effects of glass former substitution, IOX concentration and synthesis method can be made: (1) The mechanical properties decrease with increasing amount of B₂O₃+Na₂O/SiO₂, using both annealing and melt-and-quench methods(2) The mechanical moduli do not deviate much from 0% K/Na glass compositions, suggesting that IOX has limited effect to the mechanical properties of ISG series glass. (3) Both Fig. 3 and 4, shows flat curve with the increasing IOX concentration, suggesting B₂O₃+Na₂O/SiO₂ concentration has higher effect on the mechanical modulus than Na/K substitution

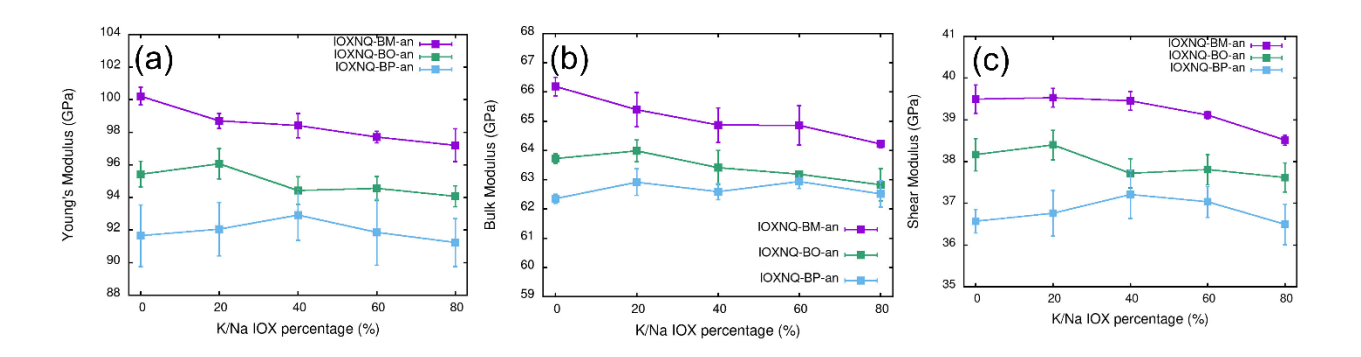


Figure 3 (a) Young's, (b) Bulk, and (c) Shear modulus of the IOXISG-an (annealed glass) series glass with increasing IOX concentration

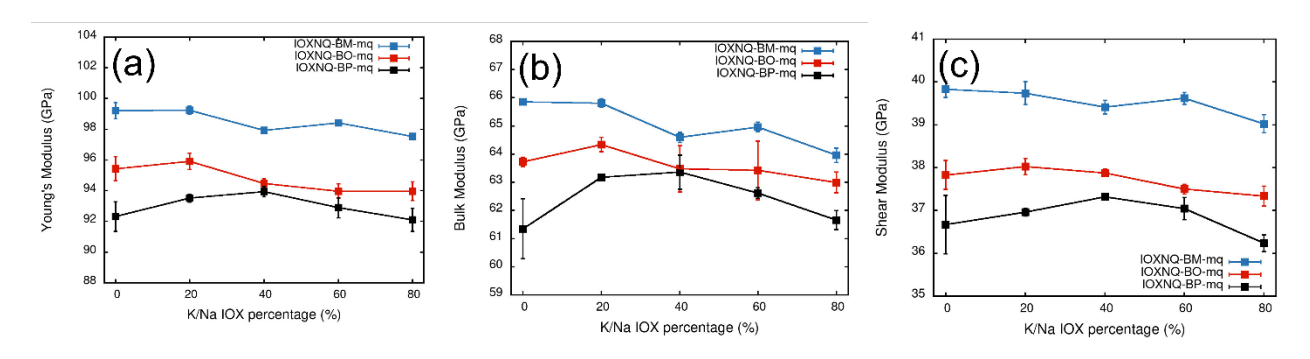


Figure 4 (a) Young's, (b) Bulk, and (c) Shear modulus of IOXISG-mq (melt and quenched) series glass with increasing IOX concentration

Fig. 5 and 6 show the mechanical moduli calculated for NQ-an and NQ-mq series of glasses, respectively. Three observations can be made: (1) The mechanical properties decrease as the Al₂O₃+Na₂O/SiO₂ substitution increases for both annealing and melt-and-quench methods. (2) Three mechanical moduli show steady increase with increasing K/Na concentration, moreover, this feature does not affect by the Al₂O₃+Na₂O/SiO₂. (3) Comparing between Fig. 5 and 6, the increasing trend of mechanical properties by IOX concentration increase is diminished by melt-and-quench method. The observation suggests the influence of IOX could be hindered by the relaxation from high temperature melting.

As a short summary, the mechanical moduli of NQ series glasses are positively correlate to Na/K concentration, and the high temperature from melt-and-quench method would lower the value via structural relaxation. On the other hand, B₂O₃+Na₂O/SiO₂ has more influence on the mechanical moduli of ISG series glasses than K/Na concentration. However, it is important to note that mechanical moduli alone cannot to be considered as an indication of compressive stress generated by IOX process.

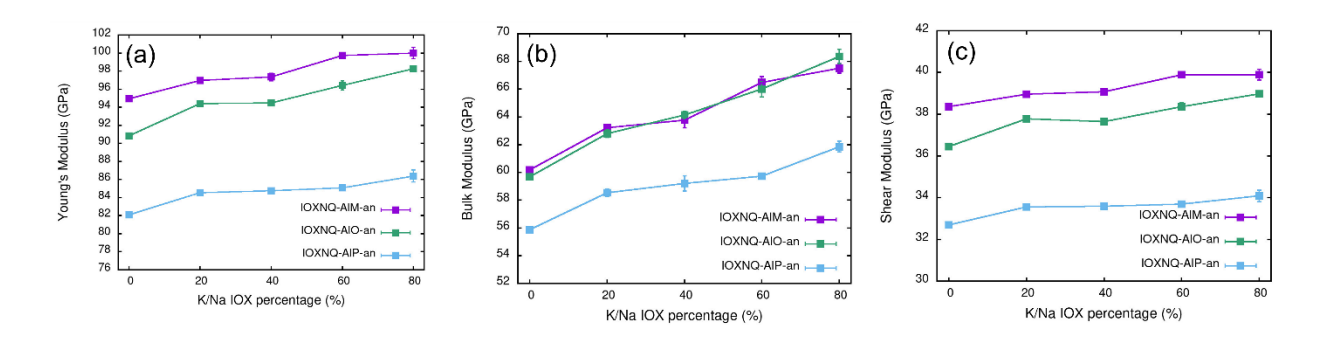


Figure 5 (a) Young's, (b) Bulk, and (c) Shear modulus of the IOXNQ-an (annealed) series glass with increasing IOX concentration

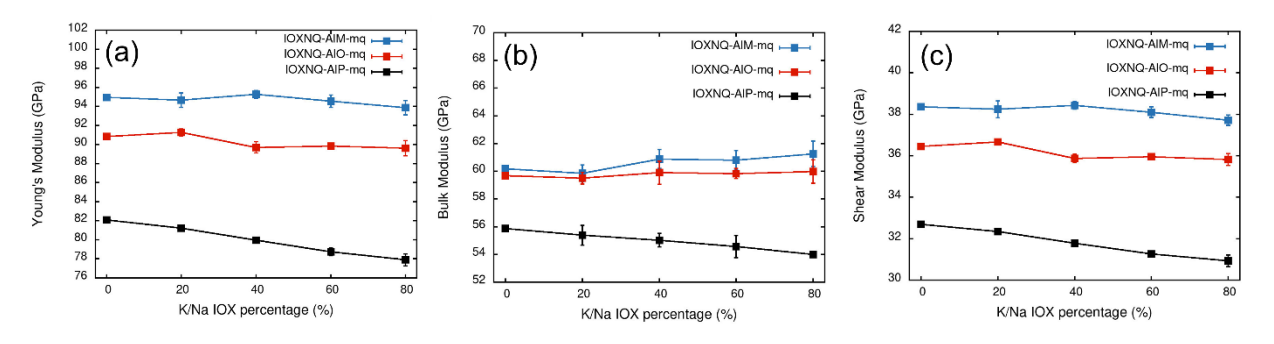


Figure 6 (a) Young's, (b) Bulk, and (c) Shear modulus of IOXNQ-mq (melt and quench) series glass with increasing IOX concentration

3.2 QSPR analysis of the mechanical properties

The correlation between the mechanical properties and the theoretical structural descriptor of (IOX)ISG-an and (IOX)ISG-mq glasses are established and shown in Fig. 7 and 8, respectively. Both Fig. 7 and 8 show good linear correlation between mechanical moduli and F_{net} . Fig. 7 shows that the data point can be roughly grouped into three regions by the value of F_{net} , which are ~480, ~490 and ~500 (kcal/mol). As listed in Table 5., these regions correspond to ISG-BP, ISG-BO, and ISG-BM, respectively. The result shows that the mechanical properties of the ISG series glasses have strong linear correlation with the structural descriptor (F_{net}). And for glasses generated by melt-and quench, in Fig. 8, the correlation coefficient between mechanical properties and F_{net} is improved in (IOX)ISG-mq glasses.

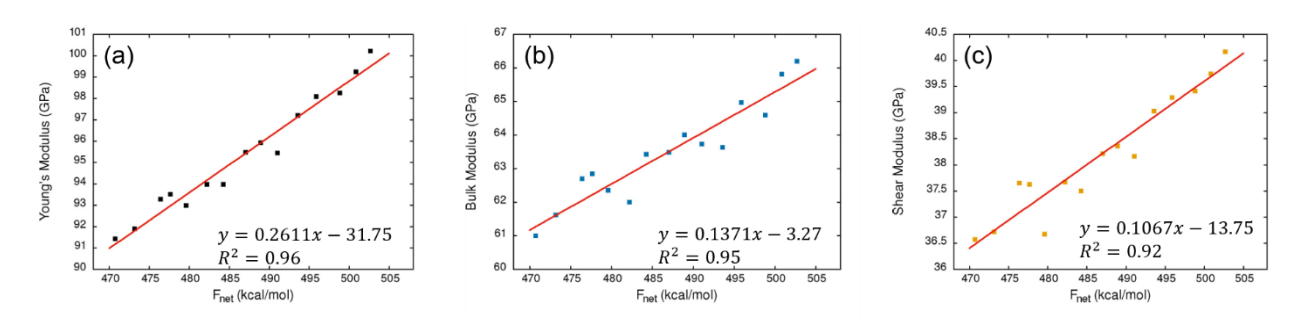


Figure 7. Correlation between the structural descriptor (F_{net}) and (a) Young's, (b) Bulk and (c) Shear modulus of (IOX)ISG-an series glass

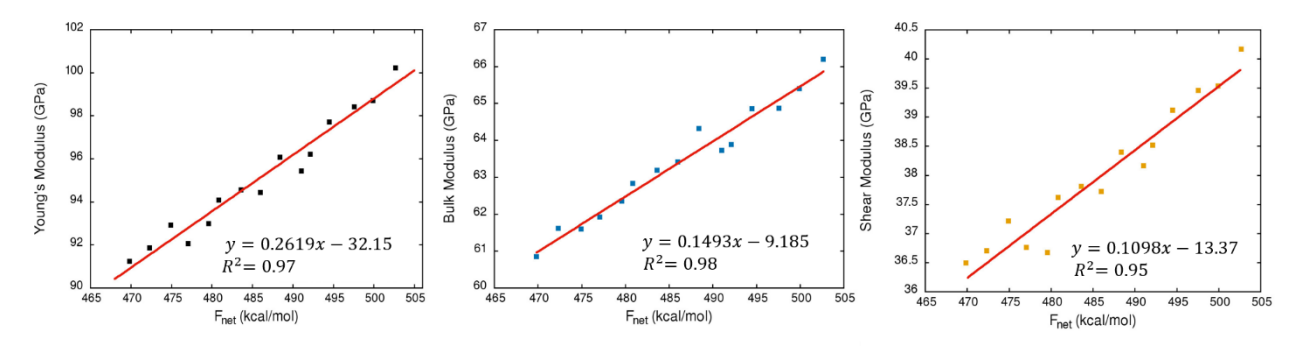


Figure 8. Correlation between the structural descriptor (F_{net}) and (a) Young's (b) Bulk and (c) Shear modulus of (IOX)ISG-mq series glass

Fig. 9 and 10 show the correlation between the F_{net} and the mechanical properties of (IOX)NQ-an and (IOX)NQ-mq glasses, respectively. The result of QSPR fitting of (IOX)NQ series glass and (IOX)ISG series glass show much poorer linear correlation, especially in comparison to those in Fig. 7 and 8 where good linear correlations were found for both the (IOX)ISG-an and -mq series of glasses. As shown in Fig. 9, the data points can be distinctively grouped into three regions by the value of F_{net} , which are ~440, ~470, ~500 (kcal/mol), as listed in Table 5. Detailed structural contribution to F_{net} can be found in Tables S1 and S2. From low to high F_{net} , these three regions correspond to NQ-AlP, NQ-AlO and NQ-AlM, respectively. Within each region, it can be seen that increasing K⁺ to Na⁺ IOX ratio results in significant increases in elastic moduli but with only small change in F_{net} . Comparing between Fig. 9 and 10, the correlation between F_{net} and mechanical properties of the (IOX)NQ-mq glasses shows better linear correlation than the (IOX)NQ-an series of glasses.

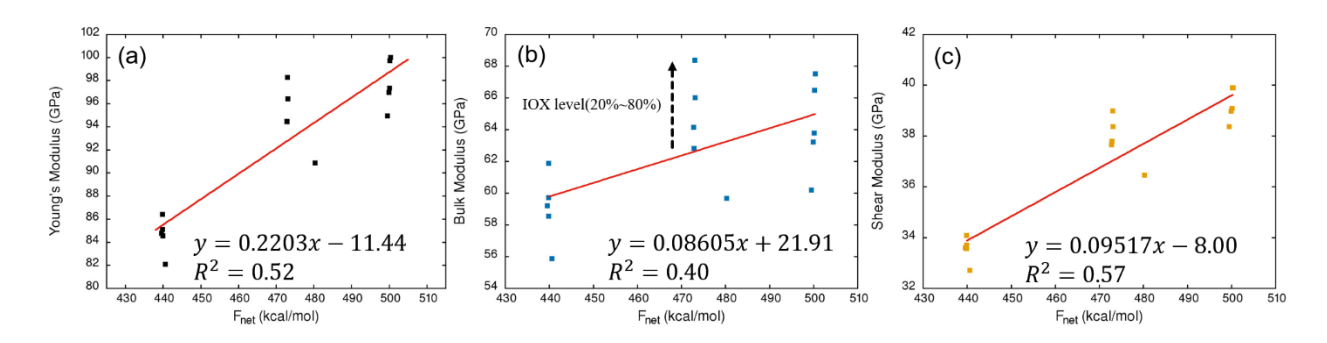


Figure 9 Correlation between the structural descriptor (F_{net}) and (a) Young's (b) Bulk and (c) Shear modulus of (IOX)NQ-an series glass

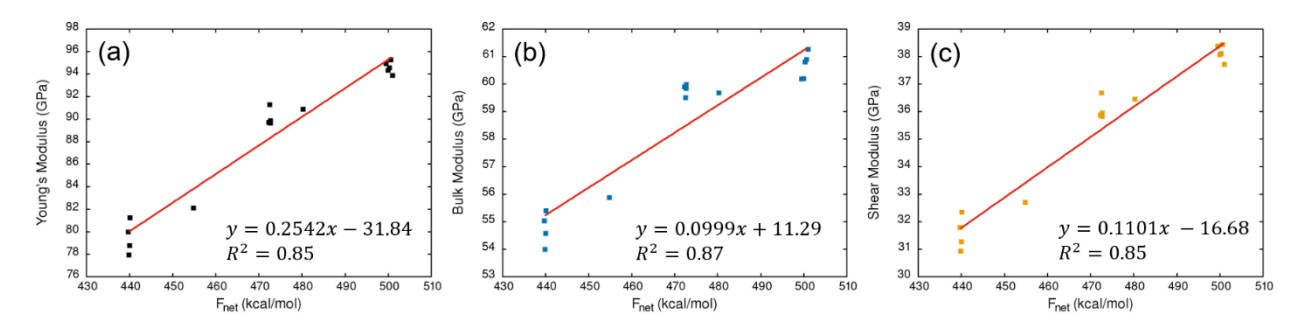


Figure 10 Correlation between the structural descriptor (F_{net}) and (a) Young's (b) Bulk and (c) Shear modulus of (IOX)NQ-mq series glass

Table 5 Theoretical structural descriptor (F_{net}) of non-IOX glasses

Glass Composition	F _{net} (kcal/mol)
ISG-BM	499.91 ± 0.15
ISG-BO	488.41 ± 0.57
ISG-BP	477.08 ± 0.48
NQ-AlM	499.97 ± 0.08
NQ-AlO	472.91 ± 0.20
NQ-AlP	439.93 ± 0.16

3.3 Linear network dilation coefficient and compressive stress

The final molar volume of ISG and NQ glasses generated by annealing and melt-and-quench as the function of IOX concentration are shown in Fig. 11 and 12, respectively. Fig. 11 shows that the molar volume of all ISG series glass increases as the IOX increases. Fig. 11-(a) to (c) shows the difference between the molar volume of glass acquired from two methods shrink as B₂O₃+Na₂O/SiO₂ substitution increases. Furthermore, the increase of molar volume of melt-and-quench glass is at a rate approximately twice than that of the anneal glass, which implies twice the

strain and LNDC. Fig. 11 also shows that some deviation from the linear function. Since the value are small, we consider the deviation to be resulted from the lack of parallel tests and the time of melting or equilibrium in MD simulation, which have high influence when investigating multi-component glasses.

Fig. 12 shows that the increase of Al₂O₃+Na₂O/SiO₂ substitution has little effect on the molar volume of NQ series glass. The increase of molar volume of NQ-mq glasses with increasing IOX concentration is also at a rate approximately twice than NQ-an glasses, which is similar to the behavior in ISG series glass. Comparing Fig 12 to Fig 11, the data deviation is smaller than ISG series glass, which gives the overall linear fitting a R² value larger than 0.9. One possible explanation is that the composition of NQ series glass is simpler than that of ISG series glass, which allows to have more prominent effect of K/Na substitution in the NQ series than in the ISG series.

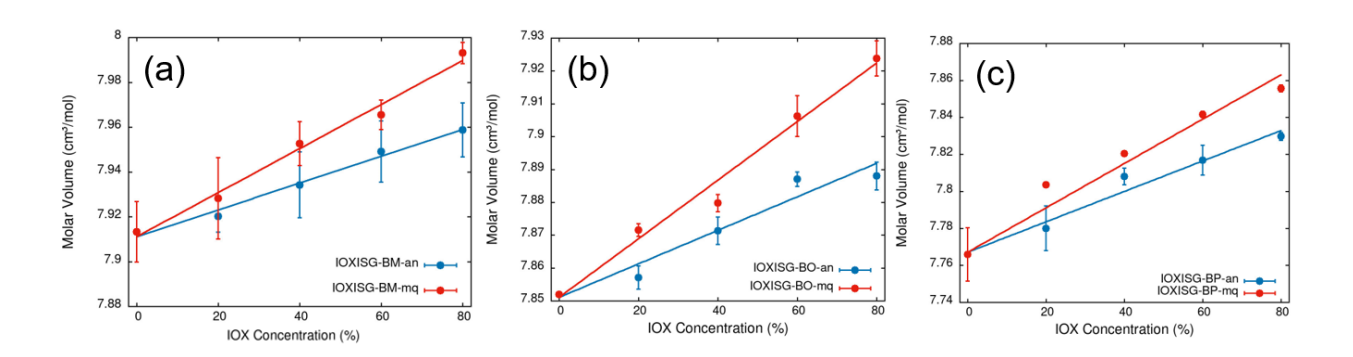


Figure 11 Influence of IOX to molar volume for the anneal and melt-and-quench in (a) ISG-BM (b) ISG-BO and (c) ISG-BP glass

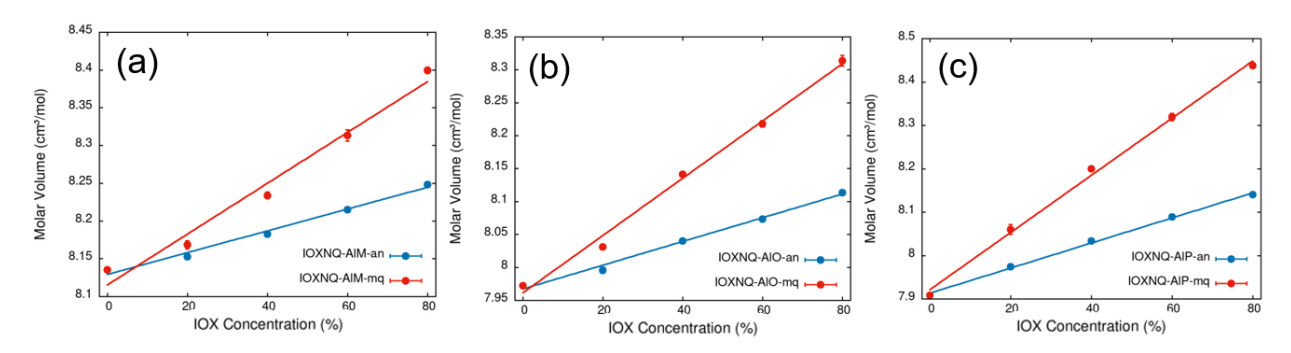


Figure 12 Influence of IOX to molar volume for the anneal and melt-and-quench in (a) NQ-AlM (b) NQ-AlO and (c) NQ-AlP glass

The LNDC of ISG and NQ series glasses were calculated by using the molar volume difference as between anneal and melt-and-quench glasses as a function of IOX concentration $(\frac{\partial V}{\partial C}$ in Eq. (2)), the results are shown in Fig. 13. Importantly, the LNDC induced in the NQ series is 3-4 times higher than those of the ISG series, suggesting that the NQ series glasses are more suitable for IOX strengthening than the ISG series. Additionally, the composition with the highest amount of glass-formers mixing (IOXISG-BP and IOXNQ-AlP) have the largest LNDC. Comparing between Fig. 13-(a) and (b), the LNDC of IOXISG and IOXNQ series glass share two similar behaviors: (1) The LNDC increases logarithmically, instead of linearly, with IOX concentration, which suggests that the strain induced by each molar of K/Na substitution is lower than the strain resulted from the previous substitution, resulting to a saturation point of strain. (2) The baseline of LNDC is mainly determined by the compositions, meaning the amount of strain induced by IOX is highly affected by the glass former substitution. In Fig 13-(a), the LNDC curve of IOXISG-BO and IOXISG-BM are close and share a same saturation point ($B \sim 0.073$ ppk/mol of K/Na) with each other. This behavior is similar to Fig 13-(b), where the LNDC of IOXNQ-AlM-an and IOX-AlO-an are close with each other. Furthermore, Fig 13-(a) and (b) shows that the LNDC values of IOXISG-BP-an and IOXNQ-AlP-an are higher than the other two glasses in the same series. The result suggests that more strain can be induced from IOX for the higher amount of Al₂O₃+Na₂O/SiO₂ in NQ series glass and higher amount of B₂O₃+Na₂O/SiO₂ in ISG series glass.

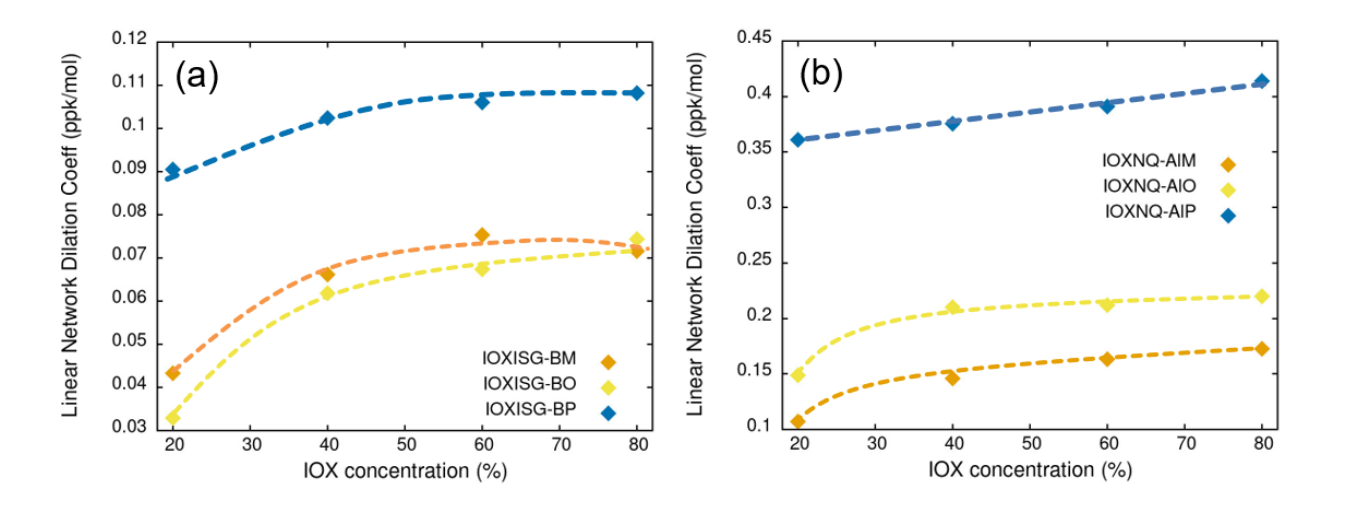


Figure 13. Linear network dilation coefficient (LNDC) of (a) ISG series glass and (b) NQ series glass as a function of increasing K/Na substitution.

4 Discussion

The MD simulation shows that the F_{net} , mechanical properties and LNDC of glasses are affected by both the glass former substitution and IOX concentration. Some behaviors corresponding to the compositional change can be found: (1) The mechanical moduli shown in section 3.1 shows three different baselines for increasing glass former substitution. Removing SiO₂ lowers the mechanical properties even with the increase of glass former per substitution. (i.e., $B_2O_3+Na_2O)/SiO_2$ for ISG series glass and $(Al_2O_3+Na_2O)/SiO_2$ for NQ series glass) (2) Despite that both ISG and NQ are borosilicate-based composition, the enhancement of mechanical properties by IOX is more evident in the NQ series glass than in ISG series glass, which can be resulted from the compositional difference. (3) The F_{net} of (IOX)NQ series glass can be divided into three different regions while no obvious data separation can be found in (IOX)ISG series glass, suggesting different ability of accommodating substituting K⁺.

Since the structural features have prominent effect on the mechanical properties, the change of Q_n species of major glass formers with glass former substitution were calculated. Here Q_n has the meaning of glass former cation polyhedron with n bridging oxygen. Originally, Q_n is specifically used for glass former cations with four-fold oxygen coordination (Q). For the complex glasses studied in this work, we have glass formers that have coordination number other than four but for simplicity we denote these as SiQ_n or BQ_n species. Particularly, we consider SiO_2 , Al_2O_3 , B_2O_3 , and ZrO_2 as glass formers so an oxygen that is linked with any of two of these glass former cations are considered to be a bridging oxygen. Fig 14-(a) and (b) show that, SiQ_4 converts to SiQ_3 ($SiQ_4 \rightarrow SiQ_3$) and BQ_4 converts to BQ_3 ($BQ_4 \rightarrow BQ_3$), while AlQ_n and ZrQ_n do not change much as the $B_2O_3+Na_2O/SiO_2$ increases in ISG series. For NQ series glass, Fig 14-(c) and (d) show the same behavior of $SiQ_4 \rightarrow SiQ_3$ and $BQ_4 \rightarrow BQ_3$ with increasing $Al_2O_3+Na_2O/SiO_2$. This decrease in the Q_n species of major glass former in ISG and NQ series glass implies the decrease in the network connectivity and mechanical properties, which explains why the baseline of mechanical moduli shown in Fig 3 and 5 is shifting lower as the compositional substitution increases.

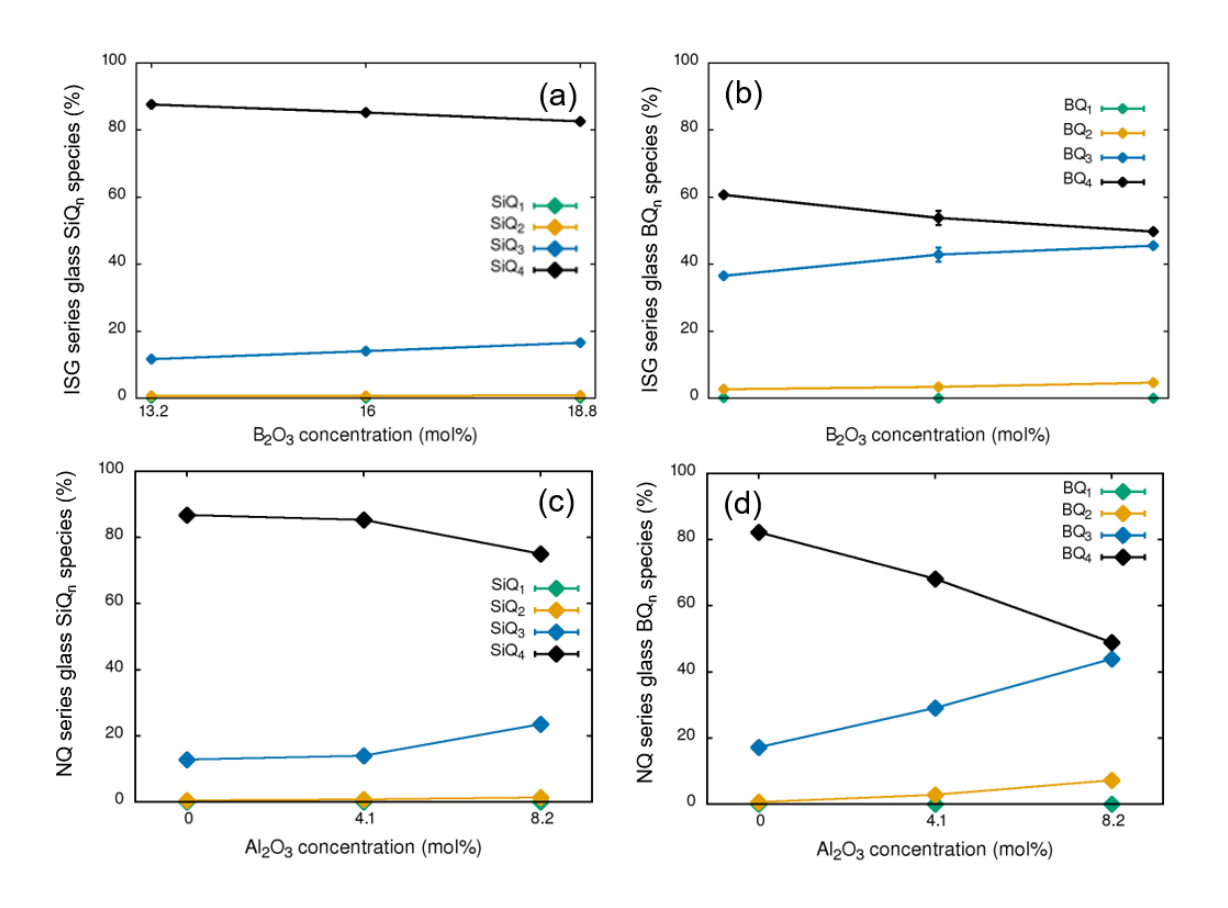


Figure 14 Q_n species of (a) Si and (b) B as a function of B₂O₃+Na₂O/SiO₂ in ISG series glass. Q_n species of (a) Si and (b) as a function of Al₂O₃+Na₂O/SiO₂ in NQ series glass.

To explain the different behavior of mechanical moduli of ISG and NQ series glass with increasing IOX concentration, we looked into the change of atomic packing fraction (APF). APF is factor that represents how "packed" the atom is in the cell, which can be considered as the amount of interatomic action requires to induce strain. The mathematical equation of APF is given by Eq. (10)

$$APF = \frac{\sum_{x}^{N_{ion}} R_{x} n_{x}}{V_{cell}}$$
 (10)

In Eq (10), the V_{cell} is the cell volume, R_x is the Shannon's radii of ion x (x = Na, Ca, Al, B^[4], B^[3], Si, Zr), and n_x is the number of x ion in the glass. Comparing between Fig 15-(a) and (b), the APF of non-IOX ISG and NQ series glass is similar, however, the APF of NQ series glass increases slightly more significant than the APF of ISG series glass with increasing IOX concentration. The

result explains the more prominent increases of mechanical moduli by IOX in NQ series glass than in ISG series glass.

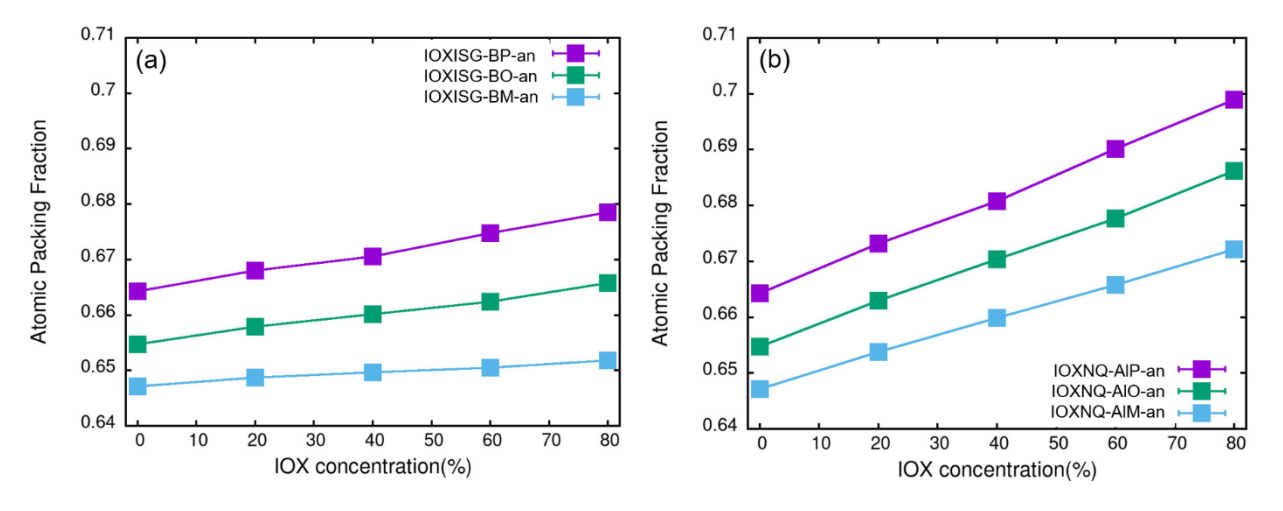


Figure 15 Atomic Packing Fraction of (a) (IOX)ISG series glass and (b) (IOX)NQ series glass

The difference in the mechanical moduli of ISG and NQ series glass can also be explained by the difference in the coordination number (CN) distribution of modifier cations K⁺ and Na⁺. As shown in Fig 16 and 17, the peak of K CN distribution in ISG-BP glass is lower than that in NQ-AlP glass, showing that the local environment of K ion is more compact in NQ-AlP than in ISG-BP glass, hence benefits the enhancement of mechanical properties in NQ series glass. On the other hand, CN distribution of K and Na does not vary much from the IOX concentration in ISG series glass, which also correspond to the limited change in APF with IOX (Fig. 15a versus Fig. 15b). The different behaviors of alkali ion CN distribution as a function of IOX concentration suggests that the structures of the multi-component ISG series glasses are more complex and have more factors involved that the NQ series. At this point, we can deduce that the glass structure of ISG series glasses are more structurally flexible than the NQ series glasses, hence the ISG series glasses are capable of accommodating the stuffing K⁺ ions and allowing them to move into positions of existing Na⁺ position without large local structural relaxations. This can be seen from parameters used for F_{net} calculations listed in Table S1 and S2. This can also explain the different trend of F_{net} in IOXISG and IOXNQ glasses (Figs. 7 and 8), which are mainly contributed by the change of K⁺ and Na⁺ contributions, instead of the local structural changes of the glass former cations (as shown in Table S1 and S2).

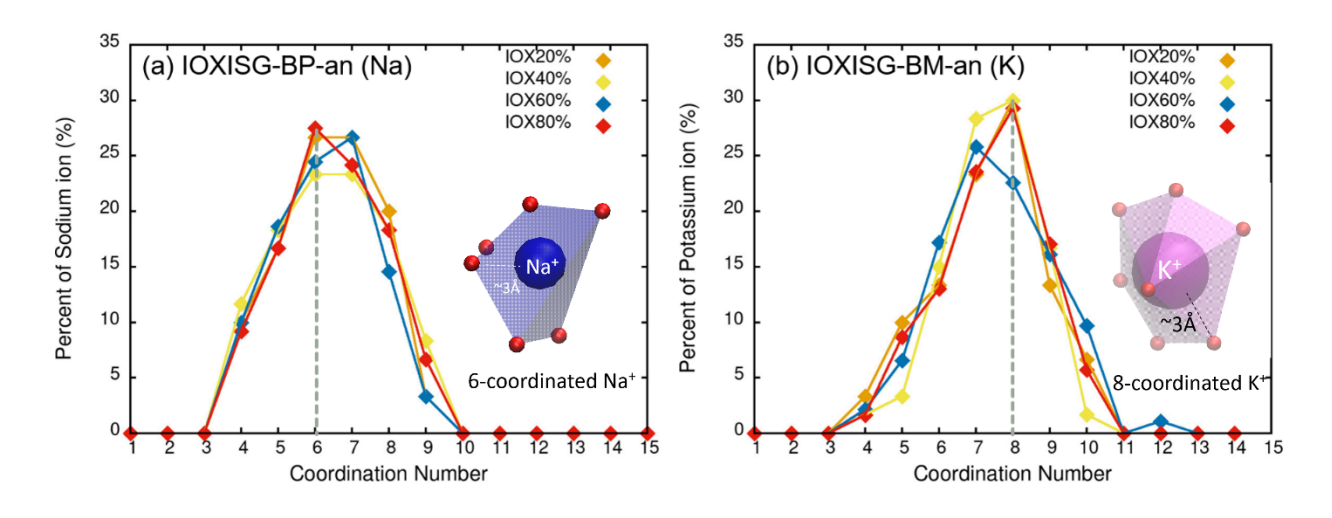


Figure 16 Distribution of (a) Na and (b) K ion coordination number and their local environment (within 3Å) of IOXISG-BP-an glass

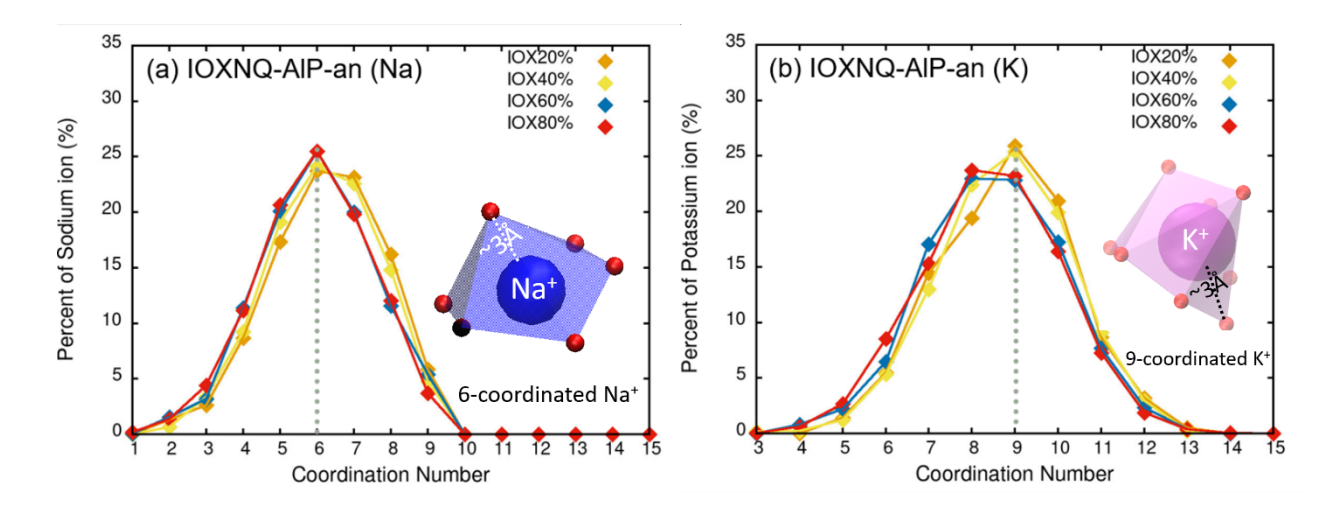


Figure 17 Distribution of (a) Na and (b) K ion coordination number and their local environment (within 3Å) of IOXNQ-AlM-an glass

Basing on the stress generated after IOX from simulations and neglecting stress relaxation, we obtained stress profile of IOX glasses. The compressive stresses generated of each glass as a function of the level of IOX were calculated based Eq. 1 and the results are shown in Fig 18. The compressive stress gradually increases with increasing K/Na concentration and show a plateau when IOX concentration reaches 40 to 60%. Moreover, similar to elastic modulus, the value of compressive stress is influenced by the glass former substitution, i.e., the overall SiO₂

concentration. Comparing to the compressive stress after IOX commercially-available Gorilla glass® (usually in the 500-800 MPa range), the compressive stress of ISG and NQ series glass are significantly lower. Furthermore, although the Young's modulus of (IOX)ISG and (IOX)NQ series glasses are in the same range of $80\sim100$ GPa (Fig. 3 and 5), the compressive stress of IOXNQ series glass is significantly larger than the IOXISG series glass. The calculated Young's moduli from MD simulations agree well with experimental values, hence the low compressive stress after IOX is mainly due to the low LNDC that is about 10 times lower than the experimental values 16,44 . This also indicates the importance of LNDC on the compressive stress generated by chemical strengthening. Importantly, the MD simulation results from this work show that LNDC strongly depends on glass composition and it cannot be considered as simply a second-order effect in the multi-component borosilicate glass. It is important to note that, in MD simulation, the small size of simulation cell can result to certain degree of compositional inhomogeneity, which can affect the C_{avg} in Eq. (1). Furthermore, it would be valuable to calculate the fracture toughness from IOX processed glass using MD simulations as that can provide further insights on the strengthening of the glass materials.

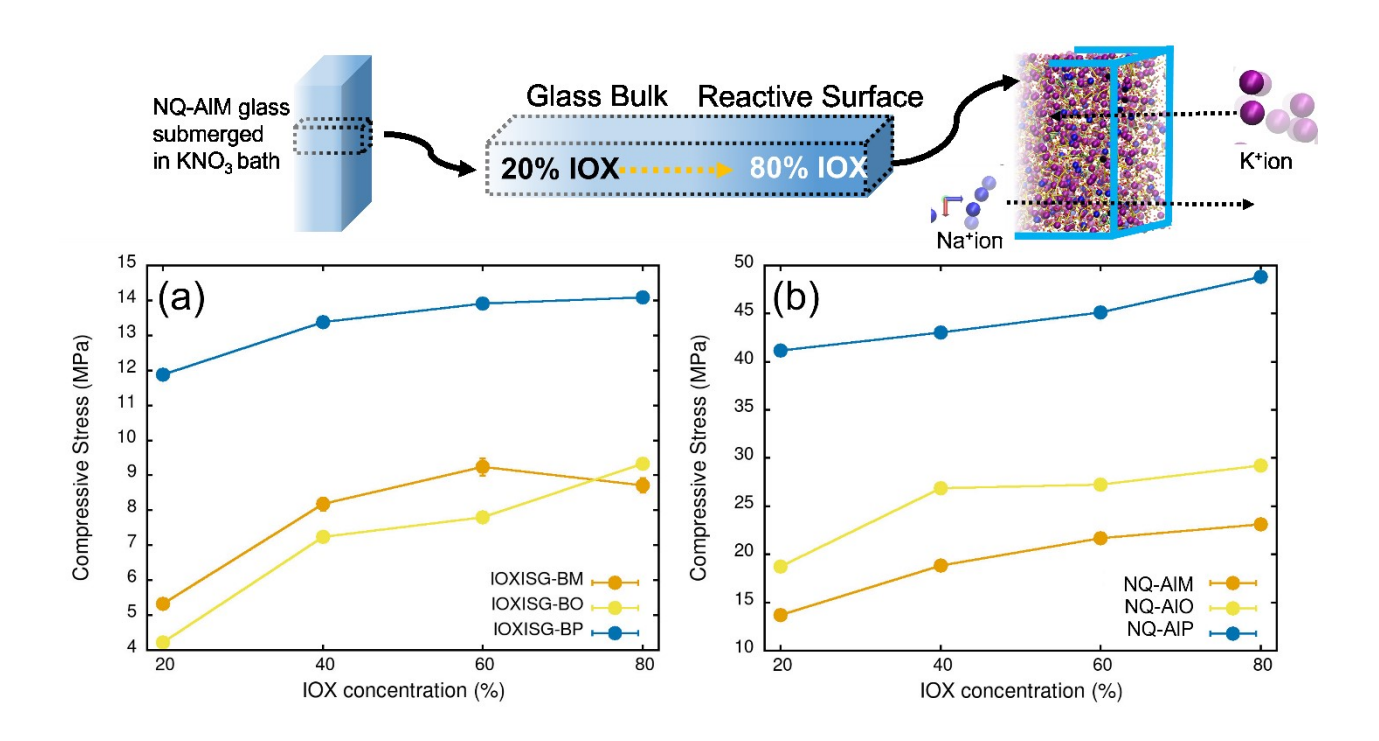


Figure 18 Schematics for the ion-exchange process of a glass and the compressive profiles of (a) IOXISG and (b) IOXNQ series glass

5 Conclusions

This study explored the glass composition effect on IOX strengthening of borosilicate glasses by using molecular dynamics based atomistic simulations and QSPR analyses. We adopted two different glass former substitutions: $B_2O_3+Na_2O/SiO_2$ substitution was performed on the one series glass and $Al_2O_3+Na_2O/SiO_2$ substitution on the other series. For each glass composition, IOX was studied with 20%, 40%, 60% and 80% of Na^+ being randomly substituted by K^+ to study the effect IOX. Structural features of these glasses, before and after IOX, and various mechanical properties were calculated. Two different methods, annealing (-an) and melt-and-quench (-mq), were used to generate the IOX glasses. The relationship between the mechanical properties and the theoretical structural descriptor (F_{net}) was established through QSPR analysis. The volume strain induced by IOX is derived by the molar volume difference between the annealing and melt-and-quench glasses, based on which the LNDC, a critical parameter for IOX, was calculated.

LNDC calculated from MD simulations shows that LNDC values are 3-4 times higher in the NQ series of glasses than in the ISG series of glasses. Also, the glasses with highest amount of mixed glass formers show the highest LNDC. As the surface compressive stress profile is largely determined by the magnitude of LNDC, NQ series of glasses show 3-4 times higher surface compressive stress than the ISG series. As a result, the NQ series of glass is much more efficient and suitable for IOX strengthening than the ISG series, which is a remarkable result from our MD simulations and IOX analysis. The results also suggest that the capability of enhancing mechanical property by IOX could be diminished by the increase of compositional complexity and decrease of network connectivity in the multi-component borosilicate glasses.

To understand the different influence of IOX to ISG and NQ series glass, detailed structural analysis from MD generated models and were performed and atomic packing factor (APF) calculated. The APF of NQ series glass increases more significantly than ISG series glass as a function of K/Na substitution. Analysis of the local environment of modifier cations shows K⁺ can be quickly accommodated in the IOX samples of ISG glass series, while K⁺ in IOX samples of NQ series of glass take a similar local environment as Na⁺. This can be explained by higher composition complexity in the ISG glass series with four oxides (SiO₂, B₂O₃, Al₂O₃, and ZrO₂) can play the role of glass former. On the other hand, the glass network in the NQ series glass series

is less accommodating that forces K⁺ ions to take similar environment of Na⁺, which leads to an increase of APT and high compressive stress. This is supported by the observation of lower strain induced and less mechanical property change induced by IOX in the ISG series glasses.

This study thus shows that combing QSPR analysis and LNDC calculated from MD simulations, the effectiveness of IOX to a glass composition can be predicted and the strengthening mechanism elucidated for complex glass compositions. They are thus a very effective way of investigating IOX strengthening of glass materials.

Acknowledgments

The authors gratefully acknowledge support of National Science Foundation (NSF) (project #1662288) and valuable discussion with Dr. Doug Allan of Corning Inc. Computational resources were provided by UNT Talon3 HPC cluster.

References:

- (1) Kistler, S. S. Stress in Glass Produced by Nonunifrom Exchange of Monovalent Ions. *Journal of The American Ceramic Society* 1962, 45 (2), 61–68.
- (2) Gy, R. Ion Exchange for Glass Strengthening. *Materials Science and Engineering B: Solid-State Materials for Advanced Technology*. March 25, 2008, pp 159–165. https://doi.org/10.1016/j.mseb.2007.11.029.
- (3) Kawamura, H.; Suzuki, R.; Matsusaka, S.; Hidai, H.; Chiba, A.; Morita, N. Formation of an Embedded Electrical Circuit in Glass Substrate by Solid-State Ion Exchange with Application of a Forward/Reverse Voltage. *Precision Engineering* 2019, *55*, 240–247. https://doi.org/10.1016/j.precisioneng.2018.09.011.
- (4) Varshneya, A. K. Chemical Strengthening of Glass: Lessons Learned and Yet To Be Learned. *International Journal of Applied Glass Science* 2010, *I* (2), 131–142. https://doi.org/10.1111/j.2041-1294.2010.00010.x.
- (5) Nordberg, M. E.; Mochel, E. L.; Garfinkel, H. M.; Olcott, J. S. Strengthening by Ion Exchange. *Journal of The American Ceramic Society* 1964, *47* (5), 216–219.
- (6) Varshneya, A. K. Fundamentals of Inorganic Glasses; Elsevier, 2013.

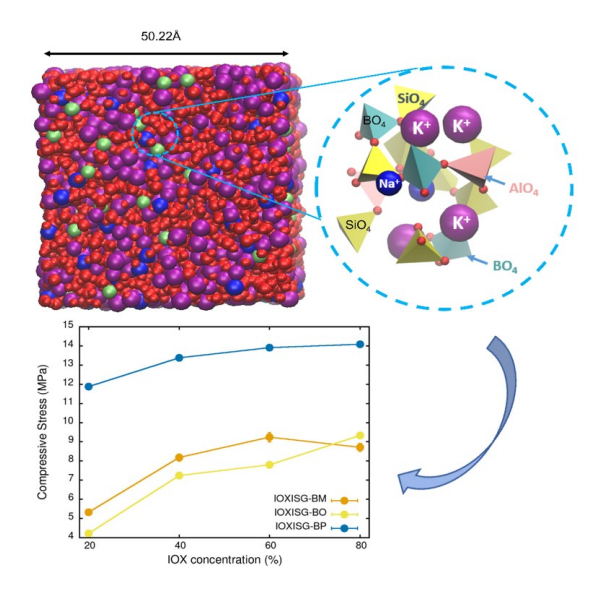
- (7) Cooper, A. R.; Krohnf, D. A. Strengthening of Glass Fibers: II, Ion Exchange. *Journal of the American Ceramic Society* 1969, *52* (12), 665–669. https://doi.org/10.1111/j.1151-2916.1987.tb04934.x
- (8) Sane, A. Y.; Cooper, A. R. Stress Buildup and Relaxation During Ion Exchange Strengthening of Glass. Journal of the American Ceramic Society 1987, 70. https://doi.org/10.1111/j.1151-2916.1987.tb04934.x
- (9) Varshneya AK, Milberg ME. Ion exchange in sodium borosilicate glasses. Journal of the American Ceramic Society. 1974 Apr;57(4):165-9. https://doi.org/10.1111/j.1151-2916.1974.tb10846.x
- (10) Soules, T. F.; Varshneya, A. K. Molecular Dynamic Calculations of A Sodium Borosilicate Glass Structure. *Journal of the American Cermaic Society* 1980, 64 (3), 145–150.
- (11) Varshneya, A. K.; Olson, G. A.; Kreski, P. K.; Gupta, P. K. Buildup and Relaxation of Stress in Chemically Strengthened Glass. *Journal of Non-Crystalline Solids* 2015, 427, 91–97. https://doi.org/10.1016/j.jnoncrysol.2015.07.037.
- (12) Macrelli, G.; Varshneya, A. K.; Mauro, J. C. Simulation of Glass Network Evolution during Chemical Strengthening: Resolution of the Subsurface Compression Maximum Anomaly. *Journal of Non-Crystalline Solids* 2019, *522*. https://doi.org/10.1016/j.jnoncrysol.2019.05.033.
- (13) Richmond, O. Theory of Residual Stress Due to Chemical Concentration Gradients.
- (14) Fu, A. I.; Mauro, J. C. Mutual Diffusivity, Network Dilation, and Salt Bath Poisoning Effects in Ion-Exchanged Glass. *Journal of Non-Crystalline Solids* 2013, *363* (1), 199–204. https://doi.org/10.1016/j.jnoncrysol.2012.12.037.
- (15) Varshneya, A. K. The Physics of Chemical Strengthening of Glass: Room for a New View. In *Journal of Non-Crystalline Solids*; 2010; Vol. 356, pp 2289–2294. https://doi.org/10.1016/j.jnoncrysol.2010.05.010.
- (16) Vargheese, K. D.; Tandia, A.; Mauro, J. C. Molecular Dynamics Simulations of Ion-Exchanged Glass. *Journal of Non-Crystalline Solids* 2014, *403*, 107–112. https://doi.org/10.1016/j.jnoncrysol.2014.07.025.
- (17) Bechgaard, T. K.; Goel, A.; Youngman, R. E.; Mauro, J. C.; Rzoska, S. J.; Bockowski, M.; Jensen, L. R.; Smedskjaer, M. M. Structure and Mechanical Properties of Compressed Sodium Aluminosilicate Glasses: Role of Non-Bridging Oxygens. *Journal of Non-Crystalline Solids* 2016, *441*, 49–57. https://doi.org/10.1016/j.jnoncrysol.2016.03.011.
- (18) Tandia, A.; Vargheese, K. D.; Mauro, J. C. Elasticity of Ion Stuffing in Chemically Strengthened Glass. *Journal of Non-Crystalline Solids* 2012, *358* (12–13), 1569–1574. https://doi.org/10.1016/j.jnoncrysol.2012.04.021.

- (19) Tandia, A.; Vargheese, K. D.; Mauro, J. C.; Varshneya, A. K. Atomistic Understanding of the Network Dilation Anomaly in Ion-Exchanged Glass. *Journal of Non-Crystalline Solids* 2012, *358* (2), 316–320. https://doi.org/10.1016/j.jnoncrysol.2011.09.034.
- (20) Mauro, J. C.; Gupta, P. K.; Loucks, R. J. Composition Dependence of Glass Transition Temperature and Fragility. II. A Topological Model of Alkali Borate Liquids. *Journal of Chemical Physics* 2009, *130* (23). https://doi.org/10.1063/1.3152432.
- (21) Katritzky, Alan R., Victor S. Lobanov, and Mati Karelson. "QSPR: the correlation and quantitative prediction of chemical and physical properties from structure." *Chemical Society Reviews* 24, no. 4 (1995): 279-287.
- (22) Kholodovych, V.; Smith, J. R.; Knight, D.; Abramson, S.; Kohn, J.; Welsh, W. J. Accurate Predictions of Cellular Response Using QSPR: A Feasibility Test of Rational Design of Polymeric Biomaterials. *Polymer* 2004, *45* (22), 7367–7379. https://doi.org/10.1016/j.polymer.2004.09.002.
- (23) Yu, X.; Wang, X.; Li, X.; Gao, J.; Wang, H. Prediction of Glass Transition Temperatures for Polystyrenes by a Four-Descriptors QSPR Model. *Macromolecular Theory and Simulations* 2006, *15* (1), 94–99. https://doi.org/10.1002/mats.200500057.
- (24) Cypcar, C. C.; Camelio, P.; Lazzeri, V.; Mathias, L. J.; Waegell, B. Prediction of the Glass Transition Temperature of Multicyclic and Bulky Substituted Acrylate and Methacrylate Polymers Using the Energy, Volume, Mass (EVM) QSPR Model. *Macromolecules* 1996, *29* (27), 8954–8959.
- (25) Mattioni, B. E.; Jurs, P. C. Prediction of Glass Transition Temperatures from Monomer and Repeat Unit Structure Using Computational Neural Networks. *Journal of Chemical Information and Computer Sciences* 2002, *42* (2), 232–240. https://doi.org/10.1021/ci010062o.
- (26) Pilania, G.; Iverson, C. N.; Lookman, T.; Marrone, B. L. Machine-Learning-Based Predictive Modeling of Glass Transition Temperatures: A Case of Polyhydroxyalkanoate Homopolymers and Copolymers. *Journal of Chemical Information and Modeling* 2019, 59 (12), 5013–5025. https://doi.org/10.1021/acs.jcim.9b00807.
- (27) Santos, C. B. R.; Lobato, C. C.; Braga, F. S.; Morais, S. S. S.; Santos, C. F.; Fernandes, C. P.; Brasil, D. S. B.; Hage-Melim, L. I. S.; Macêdo, W. J. C.; Carvalho, J. C. T. Application of Hartree-Fock Method for Modeling of Bioactive Molecules Using SAR and QSPR. *Computational Molecular Bioscience* 2014, *4* (1), 1–24. https://doi.org/10.4236/cmb.2014.41001.
- (28) Cravero, F.; Martínez, M. J.; Vazquez, G. E.; Díaz, M. F.; Ponzoni, I. Feature Learning Applied to the Estimation of Tensile Strength at Break in Polymeric Material Design. *Journal of integrative bioinformatics* 2016, *13* (2), 286. https://doi.org/10.2390/biecoll-jib-2016-286.

- (29) Linati, L.; Lusvardi, G.; Malavasi, G.; Menabue, L.; Menziani, M. C.; Mustarelli, P.; Segre, U. Qualitative and Quantitative Structure-Property Relationships Analysis of Multicomponent Potential Bioglasses. *Journal of Physical Chemistry B* 2005, *109* (11), 4989–4998. https://doi.org/10.1021/jp046631n.
- (30) Lusvardi, G.; Malavasi, G.; Tarsitano, F.; Menabue, L.; Menziani, M. C.; Pedone, A. Quantitative Structure-Property Relationships of Potentially Bioactive Fluoro Phospho-Silicate Glasses. *Journal of Physical Chemistry B* 2009, *113* (30), 10331–10338. https://doi.org/10.1021/jp809805z.
- (31) Brauer, D. S. Bioactive Glasses Structure and Properties. *Angewandte Chemie International Edition* 2015, *54* (14), 4160–4181. https://doi.org/10.1002/anie.201405310.
- (32) Lusvardi, G.; Malavasi, G.; Menabue, L.; Menziani, M. C.; Pedone, A.; Segre, U. Density of Multicomponent Silica-Based Potential Bioglasses: Quantitative Structure-Property Relationships (QSPR) Analysis. *Journal of the European Ceramic Society* 2007, *27* (2–3), 499–504. https://doi.org/10.1016/j.jeurceramsoc.2006.04.067.
- (33) Lu, X.; Deng, L.; Gin, S.; Du, J. Quantitative Structure-Property Relationship (QSPR) Analysis of ZrO 2 -Containing Soda-Lime Borosilicate Glasses. *Journal of Physical Chemistry B* 2019, *123* (6), 1412–1422. https://doi.org/10.1021/acs.jpcb.8b11108.
- (34) Lu, X.; Ren, M.; Deng, L.; Benmore, C. J.; Du, J. Structural Features of ISG Borosilicate Nuclear Waste Glasses Revealed from High-Energy X-Ray Diffraction and Molecular Dynamics Simulations. *Journal of Nuclear Materials* 2019, *515*, 284–293. https://doi.org/10.1016/j.jnucmat.2018.12.041.
- (35) Lu, X.; Du, J. Quantitative Structure-Property Relationship (QSPR) Analysis of Calcium Aluminosilicate Glasses Based on Molecular Dynamics Simulations. *Journal of Non-Crystalline Solids* 2020, *530*. https://doi.org/10.1016/j.jnoncrysol.2019.119772.
- (36) Plimpton, S. Fast Parallel Algorithms for Short-Range Molecular Dynamics. Journal of Computational Physics 1995, 117(1), 1-19. https://doi.org/10.1006/jcph.1995.1039
- (37) Deng, L.; Du, J. Development of Effective Empirical Potentials for Molecular Dynamics Simulations of the Structures and Properties of Boroaluminosilicate Glasses. *Journal of Non-Crystalline Solids* 2016, *453*, 177–194. https://doi.org/10.1016/j.jnoncrysol.2016.09.021.
- (38) Deng, L.; Du, J. Development of Boron Oxide Potentials for Computer Simulations of Multicomponent Oxide Glasses. *Journal of the American Ceramic Society* 2019, *102* (5), 2482–2505. https://doi.org/10.1111/jace.16082.
- (39) Deng, L.; Du, J. Development of Boron Oxide Potentials for Computer Simulations of Multicomponent Oxide Glasses. *Journal of the American Ceramic Society* 2019, *102* (5), 2482–2505. https://doi.org/10.1111/jace.16082.

- (40) Thompson, A. P.; Plimpton, S. J.; Mattson, W. General Formulation of Pressure and Stress Tensor for Arbitrary Many-Body Interaction Potentials under Periodic Boundary Conditions. *Journal of Chemical Physics* 2009, *131* (15), 1–6. https://doi.org/10.1063/1.3245303.
- (41) Ren, M.; Deng, L.; Du, J. Bulk, Surface Structures and Properties of Sodium Borosilicate and Boroaluminosilicate Nuclear Waste Glasses from Molecular Dynamics Simulations. *Journal of Non-Crystalline Solids* 2017, *476* (9), 87–94. https://doi.org/10.1016/j.jnoncrysol.2017.09.030.
- (42) Hill, R. The Elastic Behaviour of a Crystalline Aggregate. *Proceedings of the Physical Society. Section A* 1952, *65* (5), 349–354. https://doi.org/10.1088/0370-1298/65/5/307.
- (43) Sun, K.-H. FUNDAMENTAL CONDITION OF GLASS FORMATION*. *Journal of American Ceramic Society* 1946, *30* (9), 277–281. https://doi.org/10.1111/j.1151-2916.1947.tb19654.x
- (44) Tandia, A.; Vargheese, K. D.; Mauro, J. C.; Varshneya, A. K. Atomistic Understanding of the Network Dilation Anomaly in Ion-Exchanged Glass. *Journal of Non-Crystalline Solids* 2012, *358* (2), 316–320. https://doi.org/10.1016/j.jnoncrysol.2011.09.034.

Graphical abstract



P-H Kuo, J. Du, J. Phys. Chem. B 2022, 126, 9, 2060–2072